# Polarimetric evidence of a white dwarf pulsar in the binary system AR Scorpii

D. A. H. Buckley[1]*, P. J. Meintjes[2], S. B. Potter[1], T. R. Marsh[3] and B. T. Gänsicke[3]

**The variable star AR Scorpii (AR Sco) was recently discovered to pulse in brightness every 1.97 min from ultraviolet wavelengths into the radio regime. The system is composed of a cool, low-mass star in a tight, 3.55-hour orbit with a more massive white dwarf. Here we report new optical observations of AR Sco that show strong linear polarization (up to 40%) that varies strongly and periodically on both the spin period of the white dwarf and the beat period between the spin and orbital period, as well as low-level (up to a few per cent) circular polarization. These observations support the notion that, similar to neutron-star pulsars, the pulsed luminosity of AR Sco is powered by the spin-down of the rapidly rotating white dwarf that is highly magnetized (up to 500 MG). The morphology of the modulated linear polarization is similar to that seen in the Crab pulsar, albeit with a more complex waveform owing to the presence of two periodic signals of similar frequency. Magnetic interactions between the two component stars, coupled with synchrotron radiation from the white dwarf, power the observed polarized and non-polarized emission. AR Sco is therefore the first example of a white dwarf pulsar.**

Radio pulsars, discovered nearly 50 years ago, are fast-rotating magnetized neutron stars with spin-modulated synchrotron radio emission, powered by spin-down energy loss of fast rotating neutron stars[1]. The star AR Sco was recently discovered to be a 3.56-h close binary, containing a fast-spinning (spin period $P_s = 117.1$ s) white dwarf, showing strong brightness variations across most of the electromagnetic spectrum (ultraviolet to radio), most strongly modulated on the $P_b = 118.2$-s beat (synodic) period, and its harmonics[2]. The spin-down of the white dwarf ($\dot{P}_b = 3.92 \times 10^{-13}$ s s$^{-1}$) powers non-thermal emission, whose luminosity far exceeds (by a factor of $\geq 14$)[2] the combined luminosity of the stellar components and dominates the spectral energy distribution (SED). These observations were explained in terms of beamed synchrotron radiation from the white dwarf, some of which is reprocessed by the companion star[2]. The weak X-ray emission suggests that little accretion power is produced in AR Sco, which either implies that it is currently in a propeller mass ejection phase or there is no mass transfer at all. If the former, then it would be similar to the white dwarf in the cataclysmic variable AE Aquarii[3–6], which has a 33-s spin period and a $\dot{P} = 5.6 \times 10^{-14}$ s s$^{-1}$. However, the lack of flickering and broad emission lines in AR Sco, indicative of mass outflows which are seen in AE Aqr, implies no mass loss and suggests that a different mechanism is draining the rotational kinetic energy from the rapidly rotating white dwarf in AR Sco, perhaps similar to that operating in pulsars, namely dipole radiation[4] and magnetohydrodynamic (MHD) interactions.
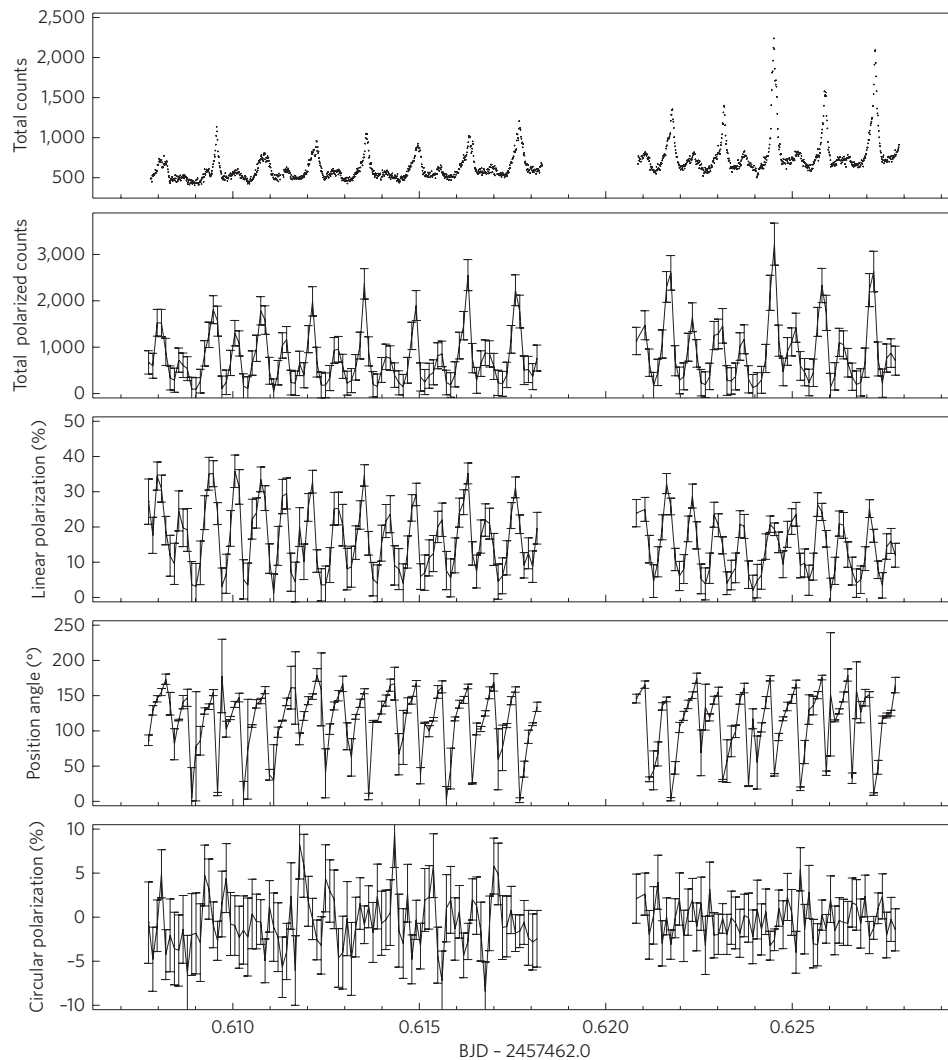
## Results

We present and explain the first polarimetric study of AR Sco, which shows strong pulsed linear polarization (up to 40%), highly modulated on the spin and beat periods, and little circular polarization (a few per cent at most). We develop a model that interprets the modulated polarized emission, as well as the earlier observations[2] of the unpolarized emission, in terms of synchrotron radiation produced at two separate sites: the magnetosphere of the magnetic white dwarf, and interaction regions involving the magnetosphere of the M-star. The combined synchrotron emission from these sites produces the pulsed emission seen at both the spin and beat periods, as well as producing a synchrotron-dominated SED.

**Photopolarimetry.** High-speed all-Stokes optical polarimetry of AR Sco was obtained using the HIPPO polarimeter[7] on the South African Astronomical Observatory (SAAO) 1.9-m telescope on two consecutive nights in March 2016 in two broad spectral bands (see Methods: Data sources). These observations revealed the system to be strongly linearly polarized, reaching levels of 40%. This is demonstrated in Fig. 1, where the flux and polarization variations in the broad red band on the first night are presented. In the Methods section, we also discuss additional observations and variations of the Stokes parameters ($I$, $Q$, $U$, $V$) on both nights. Obvious features are the strongly modulated total intensity ($I$) variations, found from a period analysis (discussed below) to be predominantly at the beat period and its harmonics, as previously reported[2]. The degree of linear polarization, $p$, shows pulse fractions up to 90%, while the position angle is seen to rotate through ~180° at the frequency of the first harmonic of the spin or beat frequency. In contrast, the level of circular polarization is comparatively low, at a few per cent, with variations in $V$ that are sometimes seen to be correlated with the $Q$, $U$ variations, when they are most strongly modulated.

**Periodicities.** The data were subjected to a period analysis (see Methods: Period analysis), and the power spectra for the Stokes $Q$ and $U$ parameters are presented in Fig. 2. We see power at both the spin ($\omega$) and beat ($\omega - \Omega$) frequencies (where $\omega$ and $\Omega$ are the spin and orbital frequencies, respectively). These results show that, as expected for a dipolar white-dwarf magnetic field, the modulation is strongest at the first harmonic of the spin period, namely 58.55 s, implying that polarized emission is seen from both magnetic poles. These results can be explained by the white-dwarf magnetic field producing a

**Figure 1 | Time-series polarimetry.** Red-band (570–900 nm) photopolarimetry of AR Sco taken on 14 March 2016. The top panel shows the total intensity, in 1-s bins, while the remaining three panels show, respectively, total polarized flux ($s$), degree of linear polarization ($p$), position angle of linear polarization ($\theta$) and the degree of circular polarization ($V/I$), all with 10-s bins. Counts in the top two panels are per time bin, and error bars are $1\sigma$. The data cover orbital phase interval $\phi = 0.10-0.23$, and the gap is when a background measurement was obtained. BJD, barycentric Julian date.

magnetically confined bipolar outflow of charged particles emitting strong linearly polarized synchrotron radiation which, together with the magnetic field of the white dwarf, sweeps across our line of sight and across the inner face of the M-star companion, where it leads to unpolarized reprocessed optical emission.

**Spin-modulated polarization.** The spin-phase-folded polarimetry is shown in Fig. 3, which clearly shows the double-peaked variations of the polarized intensity, and particularly the strongly modulated (~90% pulse fraction) linear polarization, together with the large swing in position angle through 180°, a likely consequence of viewing the dipole perpendicular to its axis. The folded data are different on the two nights, with a much higher percentage polarization and a higher pulse fraction seen on the first night. The different nature of the spin modulations on the two nights may be due to the different orbital phases of the two observations, which were at $\phi_{orb} \approx 0.15$ and $\phi_{orb} \approx 0.64$, respectively, although further observations over a number of orbital cycles will be needed to confirm this. Both the spin and beat modulations combine differently on the two nights, resulting in the variability of the waveforms for the phase-folded variations. Extracting the two pure spin and beat signals, as a function of orbital phase, will require more extensive observations,

and likewise for discriminating between repeatable orbital modulations and stochastic effects.

In Fig. 4, we plot the average $Q$ and $U$ data pairs over a white-dwarf spin cycle. We draw the trajectories of their motion in the $Q-U$ plane, which follow anticlockwise loops, and demonstrate how they vary as the magnetic orientation changes. On the first night ($\phi_{orb} \approx 0.15$), the main peak maps to the outer circle and the secondary peak maps to the lower half of the small loop inside it. For the observation on the second night ($\phi_{orb} \approx 0.64$), there is an apparent phase change and more complex polarized flux variations, leading to a different trajectory in the $Q-U$ plane, possibly indicative of a variation in the magnetic field orientation over the two nights due to orbital modulation.

These $Q$ and $U$ variations are qualitatively similar to that seen in the optical polarimetry of the Crab pulsar[8], although the latter's $p$ and $\theta$ variations show rather different morphologies, with more abrupt $\theta$ 'swings' than we see for AR Sco in our lower-resolution data. Although the polarized flux was not shown for the Crab in this study, the duty cycle of the light curve for the Crab is ~30% (for a normalized intensity $\geq 0.1$), much less than the minimum duty cycle of ~60% seen for the polarized and total ultraviolet flux[2] in AR Sco. Also, there are a range of different $\theta$ swing morphologies observed
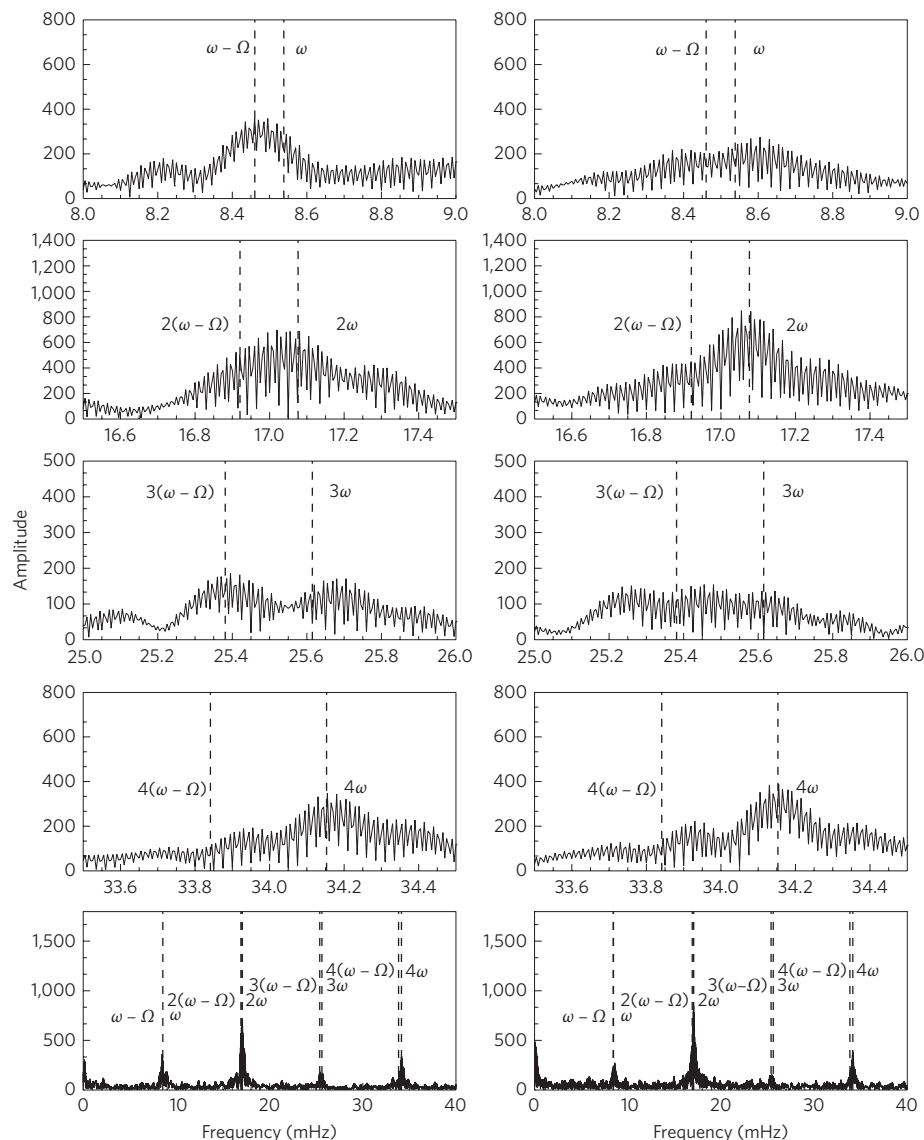
**Figure 2 | Polarimetry periodograms.** Amplitude spectra of the Stokes $U$ (left) and $Q$ (right) parameters from the two combined nights of HIPPO data, through the 'clear' filter (350–900 nm). The bottom two panels cover frequencies from 0–40 mHz (periods <25 s), while the top eight panels show the fundamental and harmonic frequencies in more detail. The dashed vertical lines mark the beat and spin frequencies ($\omega - \Omega$ and $\omega$, respectively) and their first, second and third harmonics.

in radio pulsars[9], which have been interpreted in terms of a rotating vector model[10] in which the linear polarization vector ($p$, $\theta$) represents a projection of the magnetic field in which the polarized radiation is produced on the plane of the sky. In this model the emission is confined to the magnetic poles, where the field lines of the dipole are essentially parallel to each other, with a small opening angle. The morphologies of $Q-U$ 'loop diagrams' have been used to model other magnetic systems, for example the oblique rotator model as applied to the polarized Zeeman spectra of magnetic Ap stars[11].

The polarization behaviour of AR Sco is quite different from the other polarized asynchronous magnetic white-dwarf binaries, namely intermediate polars, which, unlike AR Sco, are systems whose luminosity comes predominantly from accretion, with significant X-ray emission. In the nine intermediate polars for which polarization has been measured, it is typically only at the few percent level[12,13] and is predominantly circularly polarized, as expected from cyclotron emission from an accreting magnetic white dwarf. The high level of linear polarization and lower level of circular

polarization are consistent with synchrotron emission, for which a maximum value for the latter of ~15% is expected[14].

**Constraining the white-dwarf magnetic field.** The lack of the usual signatures for accretion, namely flickering and strong, broad and variable Doppler-broadened emission lines, coupled with the relatively low X-ray luminosity[2] (~$5 \times 10^{30}$ erg s$^{-1}$), some two orders of magnitude less than a typical accreting magnetic white dwarf, is evidence that the white dwarf in AR Sco is currently not accreting, or has a very low accretion rate. The ratio of X-ray to spin-powered luminosity ($\alpha = 3.3 \times 10^{-3}$; see Methods: Luminosities) indicates that the white dwarf in AR Sco is currently behaving as a rotation-powered pulsar, similar to AE Aqr[4] (see also Supplementary Fig. 8). Most of the luminosity of the system is being driven by rotational kinetic energy losses. The bulk of the spin-down power is expected to be lost by a combination of magnetic dipole radiation (see Methods: Magnetic dipole radiation; see also ref. [4] and references therein), as well as MHD interactions of the fast-rotating white dwarf's magnetic field with the secondary star. Additional
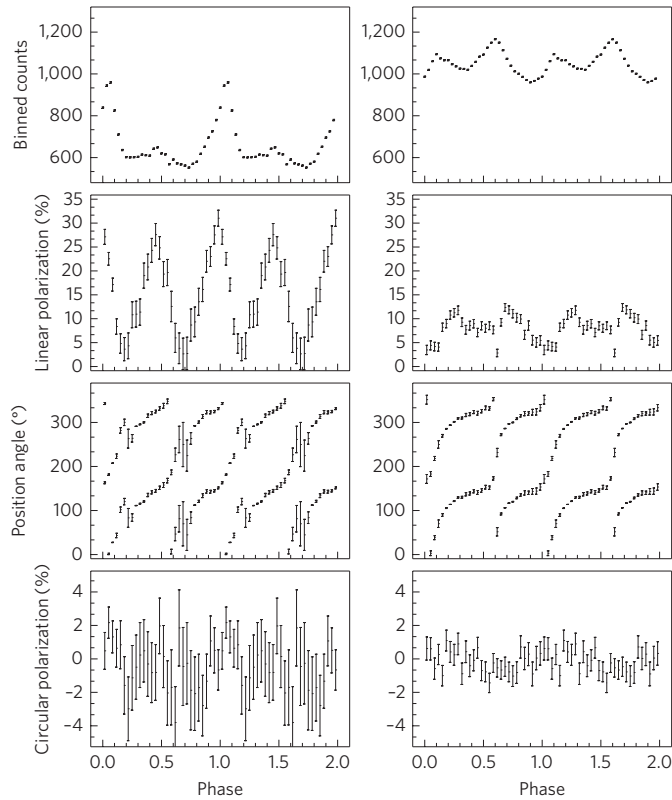
**Figure 3 | Spin-modulated polarization.** The panels show the spin-phase-folded (into 30 bins per cycle) red-band (OG 570 filter) variations for total intensity ($I$), degree of linear polarization ($p$), position angle ($\theta$) and degree of circular polarization ($v$) on the 14/15 (left panels) and 15/16 March 2016 (right panels), respectively. Two cycles are shown for clarity. Error bars are $1\sigma$.

losses may also come from an outflow of relativistic charged particles from the magnetic white dwarf and a wind from the M-star companion.

The upper limit on the magnetic dipole strength can be derived assuming that the bulk of the spin-down power is radiated by dipole radiation (Poynting radiation; see Methods: Magnetic dipole radiation). So if $L_{md} = L_{\dot{v}_s}$ (the spin-down power)[2], the upper limit placed on the white-dwarf magnetic field for a maximum dipole tilt angle to the spin axis of $\chi = 90°$ is given as

$$B_{1,*} \approx 500 \left( \frac{L_{\dot{v}_s}}{1.5 \times 10^{33}\,\text{erg s}^{-1}} \right)^{1/2} \left( \frac{P_s}{117\,\text{s}} \right)^2 \left( \frac{R_{wd}}{5.5 \times 10^8\,\text{cm}} \right)^{-3} \text{MG} \quad (1)$$

where $P_s$ and $R_{wd}$ are the spin period and radius of the white dwarf, respectively. This value is in the regime for high-field magnetic white dwarfs, either isolated or in magnetic cataclysmic variables[15].

Another approach[16], assuming that a fraction of the spin-down power is dissipated through a magnetic stand-off shock near the secondary, gave an estimate of the magnetic field of ~100 MG. If rotational energy is also dissipated through MHD pumping of the secondary star, then a constraint can be placed by estimating the MHD power dissipated in the surface layers of the secondary[17]. Dissipation will occur through magnetic reconnection and Ohmic heating, particularly in the part of the secondary star's photosphere that faces the white dwarf. This could contribute to both the observed line emission and the strong orbital photometric modulation, which is at maximum (after removal of the spin pulsations) at $\phi_{orb} \approx 0.5$[2] when the secondary star is at superior conjunction.

MHD pumping of the secondary allows an independent constraint to be set on the white dwarf's surface magnetic field strength. If the white-dwarf magnetic field lines sweep periodically across the secondary star, the penetration depth of the magnetic flux into the surface layers is[17] $\delta = \sqrt{2\eta_{tur} / \omega_b}$ (Methods: Spin-down torque), where $\eta_{tur}$ and $\omega_b$ are the turbulent diffusivity and beat (synodic) angular frequency, respectively. For the photospheric conditions of a M-type dwarf, $\delta \approx 10^8$ cm, using[17] $\eta_{tur} \lesssim 10^{15}$ cm$^2$ s$^{-1}$. The power dissipation of magnetic energy through reconnection and Ohmic heating can be estimated from $P_{MHD} = (B^2/8\pi)(4\pi R_2^2 \delta)\, \omega_b$ (see for example ref. [17] and references therein).

For a 500-MG magnetic white dwarf, the field strength at the distance of the secondary (at a distance of $a = 8 \times 10^{10}$ cm; see Methods: Binary parameters) will be 160 G. This implies $P_{MHD} = 4 \times 10^{31}$ erg s$^{-1}$, which is ~30% of the average optical luminosity of AR Sco in excess of the combined stellar contributions[2], namely $L_+ = 1.3 \times 10^{32}$ erg s$^{-1}$. The equation for power dissipation through MHD pumping can then be expressed as:

$$B \approx 160 \left( \frac{P_{MHD}}{4 \times 10^{31}\,\text{erg s}^{-1}} \right)^{1/2} \left( \frac{R_2}{2.5 \times 10^{10}\,\text{cm}} \right)^{-1} \left( \frac{\delta}{10^8\,\text{cm}} \right)^{-1/2}$$
$$\left( \frac{P_b}{118\,\text{s}} \right)^{1/2} \text{G} \quad (2)$$

implying a dipole surface magnetic field of

$$B_{1,*} = B (a / R_{wd})^3 \leq 500 (B/160\ \text{G})$$
$$(a/8 \times 10^{10}\,\text{cm})^3 (R_{wd}/5.5 \times 10^8\,\text{cm})^{-3}\ \text{MG} \quad (3)$$

where it was assumed that the secondary star fills, or nearly fills, its Roche lobe, so equals $R_{L,2}$ (see Methods: Binary parameters). If other processes are also responsible for the line emission and heating of the secondary, for example beamed synchrotron radiation, dipole radiation or charged particles, all from the white dwarf, then this will lower $P_{MHD}$ and hence the estimate of $B$ and $B_{1,*}$ based on MHD interactions alone.

**The white dwarf pulsar.** We propose that the highly asynchronous binary system AR Sco contains a strongly magnetic white dwarf, probably having been spun-up to the current short rotation period ($P_s = 117$ s) by accretion torques during a high mass-transfer phase in its history, as has also been proposed[4–6] for AE Aqr. The observed ratios of X-ray to spin-power luminosities for AR Sco and AE Aqr[2,4] are very similar to spin-powered neutron-star pulsars[18] (see also Supplementary Fig. 8), making both of them analogous to spun-up radio pulsars[4,19]. Similarly, considering that the 70% pulse fraction of the luminosity in excess of the combined stellar components[2] is predominantly optical synchrotron emission, this implies that the synchrotron power in AR Sco is $0.06P_{sd}$, similar to the ratio of synchrotron-produced gamma-ray emission to spin-down power reported recently for a sample of spun-up gamma-ray-emitting millisecond radio pulsars[20].

The high level of linear polarization in AR Sco is consistent with synchrotron emission of relativistic electrons in ordered magnetic fields[14]. The periodicities, at both the white-dwarf spin and the beat periods, are also consistent with this emission being produced in the white-dwarf magnetosphere, which is additionally modulated at the binary period.

The SED in AR Sco[2,21] shows a $S_\nu \propto \nu^{\alpha_1}$ ($\alpha_1 \approx 1.3$) self-absorbed power-law spectral distribution for $\nu \lesssim 10^{12} - 10^{13}$ Hz, that is, at infrared to radio wavelengths. We suggest that these originate from pumped coronal loops of the nearly Roche-lobe-filling secondary star[22–24]. The magnetospheric flux tubes of the secondary star are distorted by the fast-rotating white dwarf dipolar field (see Methods:
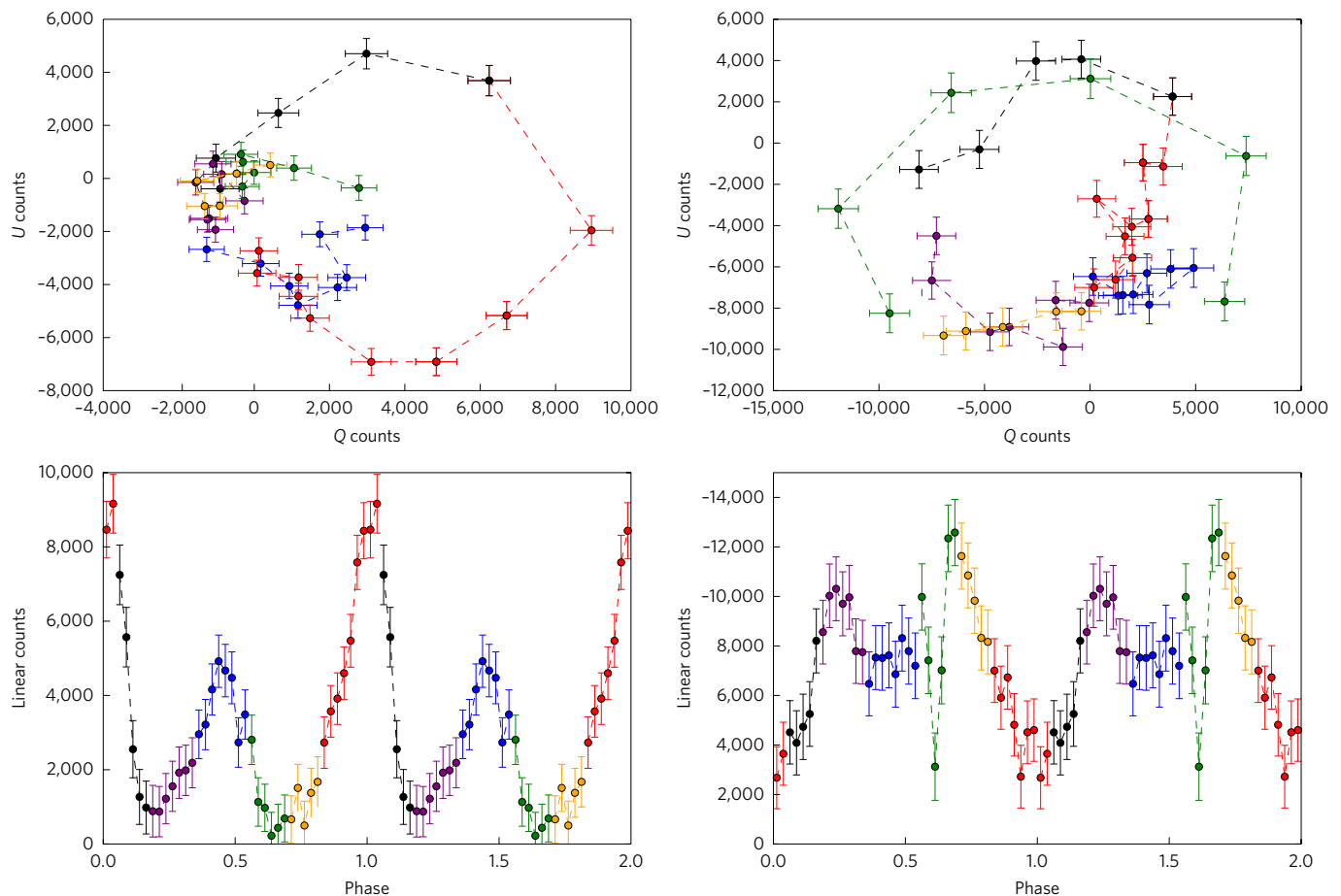
**Figure 4 | Stokes parameters *Q*, *U* and polarized flux variations over spin period.** Spin-phase-folded Stokes *Q* and *U* parameters (upper panels) and total linearly polarized flux (lower panels) for the red band (570–900 nm) are shown for the two nights 14 and 15 March 2016. The migration of the Stokes *Q* and *U* amplitude pairs is shown, plotted every 3 s, and 40 points are plotted per spin cycle. Points are colour-coded as in the average phase-folded linearly polarized flux plots. The *Q*, *U* pairs follow anticlockwise trajectories.

Magnetic interactions), inducing strong field-aligned potentials[25,26], resulting in synchrotron flares through the van der Laan process[5,27,28], whose superposition produces the observed power law at $\nu \leq 10^{12}$ Hz and the peak emission at $\nu_{\text{crit}} \approx 0.3\nu_{\text{syn}} \leq 10^{13}$ Hz. This emission is expected to be pulsed at the beat frequency, consistent with the Australia Telescope Compact Array observations[2] at 5.5 and 9.0 GHz, and may be linearly and/or circularly polarized, depending on the orientation of the flux tubes relative to the observer.

At higher frequencies, $\nu \geq \text{few} \times 10^{14}$ Hz (optical–ultraviolet–X-ray), the SED follows a different $\nu^{\alpha_2}$ power law[2], clearly distinguishable from the spectral components of both the M5 secondary and the white dwarf, where $\alpha_2 \approx -0.2$ (also see ref. [21]). This component is produced by non-thermal synchrotron emission from the magnetic white-dwarf dipole and shows a high level of linear polarization.

The absence of accretion, and hence conducting plasma, allows the induction of significant electrical potentials[29] of the order of $\Delta V_e \approx 10^{12}$ V in the vicinity of the light cylinder, $r_{\text{lc}} \approx 6 \times 10^{11}$ $(\omega_{\text{wd}}/0.054 \text{ rad s}^{-1})$ cm, which is ~7.5 times greater than the orbital separation, where the white dwarf magnetic field is of the order $B_{\text{lc}} \approx 0.4$ G. This electric field can produce a relativistic wind of electrons (and ions), with energies of the order of $\gamma_e \approx 10^6$, which will emit synchrotron radiation at frequencies up to $\nu_{\text{syn}} \leq 3 \times 10^{17}(B_{\text{lc}}/0.4 \text{ G})$ $(\gamma_e/10^6)^2$ Hz (soft X-rays) in the vicinity of the light cylinder radius. Since the whole binary system is inside the accelerator zone (that is, the light cylinder radius; see Methods: Binary parameters), this emission may be modulated at both the spin and beat periods.

If the white dwarf is an oblique rotator, with the magnetic dipole tilted relative to the spin axis, the rotating magnetosphere is expected to produce a relativistic outflowing MHD wind outside the light cylinder, with alternating regions of opposite polarity — a 'striped' wind[30–32] (see Methods: Pulsar-like particle acceleration), resulting in additional particle acceleration through magnetic reconnection and associated pulsed incoherent polarized synchrotron emission[30,31]. The emission will be pulsed at the spin period (fundamental and first harmonic, arising from both magnetic poles), as well as displaying the 180° swing of the position angle of the polarization (see previous work[32] for a discussion). The binary motion of the system may also impart a beat period modulation, seen in both the polarized and unpolarized optical emission.

## Discussion

The high degree of asynchronism in AR Sco ($P_s/P_{\text{orb}} = 0.009$) indicates a previous spin-up phase of the white dwarf, owing to a higher mass-transfer rate, similar to other highly asynchronous intermediate polar magnetic cataclysmic variables, such as AE Aqr, DQ Her, XY Ari and GK Per[33]. These systems are still undergoing mass transfer but are now likely to be in, or close, to spin equilibrium. For AE Aqr, it has been shown[34,35] that during a high mass-transfer phase the secondary star may have shed its outer envelope in a catastrophic run-away mass-transfer process, resulting in the white dwarf being spun-up to a period close to its current value of ~33 s. There is currently no observational evidence that AR Sco has evolved through such an extreme high mass-transfer phase, and so

the evolutionary path that AR Sco took to its current configuration is still an open question.

Given the high magnetic fields that we are estimating, AR Sco presents a problem when it comes to spinning up the white dwarf in the first place, since material will tend to be ejected rather than accreted, except at very high accretion rates. Since the observed white-dwarf spin-down timescale[2] of $\sim 10^7$ yr is less than the spin–orbit synchronization timescale of $\sim 2.5 \times 10^8$ yr, calculated for MHD torques alone (Methods: Spin-down torque), this implies the bulk of the spin-down power is dissipated through magnetic dipole radiation and other channels. The high value of the magnetic field is therefore the reason for the current large spin-down rate, through the various mechanisms (for example dipole radiation, MHD interactions) we have described here, which rob the white dwarf of its angular momentum.

The strongly pulsed polarized optical emission in AR Sco is analogous to that observed in pulsars, like the Crab. The ratio $\alpha = (L_x / L_{sd}) \approx 10^{-3}$ (where $L_x$ and $L_{sd}$ are X-ray and spin-down luminosities) derived for AR Sco implies that most of the luminosity of the system is not produced by accretion of matter, but by spin-down energy loss, implying that the white dwarf behaves like a spin-down powered pulsar (Supplementary Fig. 8). Electric potentials $\Delta V$ of the order $\sim 10^{12}$ V can be induced between the white dwarf and the light cylinder (Methods: Magnetic field interactions), accelerating particles to energies of the order of $\gamma_e \approx 10^6$ (Methods: Pulsar-like particle acceleration), resulting in pulsed and strongly polarized synchrotron emission, possibly up to to X-ray frequencies. However, we argue that a striped relativistic MHD wind, outside the light cylinder, may also be present (Methods: Pulsar-like particle acceleration). The pulsed emission below optical frequencies (that is, radio) arises from synchrotron emission in pumped coronal loops of the secondary star, which is consistent with the observed SED[2,21]. Future observations, particularly at X-ray and radio wavelengths, will be important in determining the exact nature of the emission mechanisms operating in AR Sco. More extensive time-resolved polarimetry will also help to disentangle the two closely spaced polarized signals, at the spin and beat period, leading to more definitive conclusions regarding geometry.

## Methods

**Data sources.** The data presented in this paper arise from observations taken at the SAAO using the 1.9-m telescope. High-speed photopolarimetry of AR Sco was conducted utilizing the HIPPO photopolarimeter on two consecutive nights, on 14 and 15 March 2016 (see Supplementary Table 1 for observing log). HIPPO is a two-channel all-Stokes photon-counting photopolarimeter[36] which records all observations as intensity measurements every millisecond. Rotating half- and quarter-waveplates modulate the signal at 10 Hz, and the data are accumulated in 100 bins per waveplate rotation. The Stokes parameters are then determined by a Fourier decomposition of the modulated signal — the $4\theta$ and $8\theta$ terms determining $Q$ and $U$, and the $6\theta$ term determining $V$ (note that $\theta$ here should not be confused with the position angle of linear polarization). The total intensity (Stokes $I$) data were post-processed by summing the millisecond measurements to a time resolution of 1 s. Likewise, the 100-ms polarization arrays were summed to a time resolution of 10 s. Calibration observations of the polarized standard star[37] HD160529 were observed on both nights to determine the zero points for both waveplate angles. In addition, an observation was made of a nearby star, $\sim 40$ arcsec northeast of AR Sco, to estimate the level of background polarization.

Simultaneous observations were undertaken in two broad wavebands defined by the convolution of the intrinsic response of the GaAs photomultipliers with the respective filters used. For both observations we used a clear fused silica filter (essentially no filter) and a Schott OG 570 glass filter, respectively, for the two channels. Channel 1 had a bandpass of 350–900 nm, while channel 2 covered 570–900 nm. All of the data were converted to Barycentric Julian Date using the accurate prescription presented elsewhere[38]. In Supplementary Figs 1 and 2 we show the variation of the Stokes parameters $I$, $Q$, $U$ and $V$ for the broadband filter on both nights, while in Supplementary Figs 3 to 6 we show the polarized flux ($s$), degree of linear polarization ($p$) and position angle ($\theta$) for both nights and both filters.

**Period analysis.** The reduced HIPPO photopolarimetry was analysed using a discrete Fourier transform periodogram program. The two consecutive nights of data (14 and 15 March) were combined and power spectra derived for

(i) the Stokes $Q$ and $U$ parameters (Fig. 2), (ii) the total and polarized intensity, (iii) the degree of linear polarization ($p$) and the position angle of the linear polarization: that is, the E-vector ($\theta$). The periodograms suffer from significant aliasing due to the relatively short spin (117.1 s) and beat (118.2 s) periods, which are unresolved on single nights, and because of the $\sim 24$-h data gap, which results in ambiguity in cycle count.

Just as was seen in the original study[2] for the $g'$ band variability, the total intensity ($I$) varies predominantly at the beat frequency and its first harmonic (Supplementary Fig. 7, right panels), with the latter being the stronger of the two. In addition, the harmonic of the spin frequency is also clearly seen, but at a lower power than for the beat harmonic. The power spectra of the ultraviolet light curves derived from the Hubble Space Telescope observations[2], although strongly aliased, clearly show that the power in the first harmonics of the spin and beat frequencies are approximately equal, implying that the white dwarf's magnetic field is directly (through beaming) or indirectly (through reprocessing) modulating the ultraviolet emission. In the case of the polarized flux (Supplementary Fig. 7, left panels), we see a broad spread of power at the first harmonic, consistent with power at both spin and beat harmonic frequencies. In the case of the third harmonics, the spin component ($4\theta$) dominates, at 29.3 s. The fact that the power of the spin-modulated polarized flux and $p$ is less than for the beat modulation is attributed to the modulation of $I$ occurring at two closely spaced periods (beat and spin), while $Q$ and $U$ vary predominantly at the spin period. Thus any calculation involving $Q$, $U$ and $I$ (as for $p$) will introduce some additional power at the beat period.

**Binary parameters.** AR Sco consists of a magnetic white dwarf and an M5 dwarf star orbiting one another with an orbital period of $P_{orb} = 3.56$ h. The pulsations observed from the ultraviolet to the radio show a double-peaked pulse profile, predominantly at the beat period $P_b$, implying that the secondary star must be a site for spin-modulated reprocessing. Furthermore, narrow line emission is seen which clearly follows the orbital motion of the secondary star and is situated near the L1 point. Based on the limits placed, the white dwarf has a mass of $M_1 \approx 0.8 M_\odot$, while the secondary star has a mass of about $M_2 \approx 0.3 M_\odot$ and therefore a mass ratio of $q = (M_2/M_1) = 0.375$. Sinusoidal variations in the optical/infrared light suggest that the secondary star is being irradiated, with its hotter/brighter side facing the white dwarf, which is best seen at orbital phase $\phi_{orb} = 0.5$ (superior conjunction of the secondary).

Assuming that the secondary is close to filling its Roche lobe, then the standard relationship[39] between the Roche-lobe size of the secondary ($R_{L,2}$) and binary separation ($a$), applicable to binaries in the range $0.3 < q < 20$ is given by $R_{L,2}/a = 0.38 + 0.2 \log q$. For AR Sco ($q = 0.375$), the orbital separation $a \approx 8 \times 10^{10}(M_{wd}/0.8 M_\odot)^{1/3}(P_{orb}/3.56 \text{ h})^{2/3}$ cm. Thus the Roche-lobe radius of the secondary star is estimated to be $R_{L,2} \approx 0.3a \approx 2.53 \times 10^{10}$ cm. The distance, $b1$, of the L1 region from the white dwarf primary can be estimated from the relation $(b1/a) = 0.5 - 0.227 \log q$ (for $0.1 < q < 10$)[40], resulting in $b1 \approx 0.6a \approx 5 \times 10^{10}$ cm. In comparison, the radius of the light cylinder, where the white dwarf's magnetosphere co-rotates with the speed of light ($c = \omega_{wd} r_{lc}$), is of the order of $r_{lc} \approx 6 \times 10^{11}(\omega_{wd}/0.054 \text{ rad s}^{-1})$cm, implying that the binary system is inside the light cylinder of the white dwarf pulsar.

**Luminosities.** It has been found[2] that the white dwarf in AR Sco is currently spinning down on a timescale of $\tau_{sd} = (\nu_s / \dot{\nu}_s) \approx 10^7$ yr. The spin-down luminosity, assuming a $0.8 M_\odot$ white dwarf, is of the order of $L_{\dot{\nu}_s} = -4\pi^2 I \nu_s \dot{\nu}_s = 1.5 \times 10^{33}$ erg s$^{-1}$ (where $I$ is the moment of inertia). The X-ray luminosity is $L_x = 4.9 \times 10^{30}$ erg s$^{-1}$, implying $\alpha = (L_x / L_{\dot{\nu}_s}) = 3.27 \times 10^{-3}$. This is very similar to the ratio found in spin-powered pulsars as well as the white dwarf in the cataclysmic variable system AE Aquarii (Supplementary Fig. 8), which has a ratio $\alpha \approx 10^{-3}$, where $L_x \approx 5 \times 10^{30}$ erg s$^{-1}$ and $L_{\dot{\nu}_s} = 6 \times 10^{33}$ erg s$^{-1}$ (see for example refs [4,5,26]).

**Magnetic dipole radiation.** The luminosity coming from magnetic dipole radiation (also known as Poynting flux) in AR Sco is given as:

$$L_{md} = \frac{2B_{1,*}^2 \omega_{wd}^4 R_{wd}^6 \sin^2\chi}{3c^3} \quad (4)$$

where $B_{1,*}$, $\omega_{wd}$, $R_{wd}$ and $\chi$ represent the surface polar field of the white dwarf, the white dwarf's spin angular velocity and radius, and the angle between the spin and magnetic axes. For our calculations of luminosities we used the Hamada–Salpeter relation to determine that the white dwarf has a radius of $R_{wd} \approx 5.5 \times 10^8 (M_{wd}/0.8 M_\odot)^{-0.8}$cm.

Re-arranging this equation to determine the magnetic field strength gives:

$$B_{1,*} \sin\chi = \left( \frac{3c^3 L_{\dot{\nu}_s} P_{wd}^4}{2(2\pi)^4 R_{wd}^6} \right)^{1/2} \quad (5)$$

**Spin-down torque.** It has been shown[41–43] that the rate of dissipation of magnetic energy in the surface layers of a cataclysmic variable secondary star of depth $\delta$ (skin-depth) is given by $\dot{W} = (B^2/8\pi)(4\pi R_2^2 \delta) \omega_b$, where $B$ is the estimated magnetic field of the white dwarf at the distance of the secondary star, $\omega_b$ is the beat-period

angular frequency of the white dwarf (essentially the same as the spin angular frequency in AR Sco), and $\delta = \sqrt{2\eta_{tur}/\omega_b}$ represents the dissipation depth of magnetic energy, where $\eta_{tur}$ is the turbulent plasma resistivity.

The total magnetic torque exerted on the secondary star, $T_D = (\dot{W}/\omega_b)$, results in a synchronization timescale which is given by $t_{syn} = I\omega_b/T_D$, where $I$ is the moment of inertia of the white dwarf, which is of the order of $I \approx 1.5 \times 10^{50}$ g cm$^2$. If we assume a 500-MG dipolar magnetic field for the white dwarf (the upper limit derived from the dipole radiation), the field strength at the distance of the secondary star is $B_{b1} \approx 160$ G. For $\delta \approx 10^8$ cm, using[17] $\eta_{tur} \leq 10^{15}$ cm$^2$ s$^{-1}$, the magnetic torque exerted on the secondary star is of the order $T_D = (B_{1,s}^2/8\pi)(R_{wd}/a)^6(4\pi R_2^2 \delta) \approx 10^{33}$ erg (=$10^{33}$ dyn cm). The resulting timescale for spin-synchronization through MHD torques for a 500-MG white dwarf is therefore $t_{syn} \approx 2.5 \times 10^8$ yr. This supports the notion that the magnetic dissipation in the thin surface layers of the secondary star ($\delta \approx 0.004 R_{L,2}$) will contribute to the dissipation of rotational kinetic energy of the white dwarf, together with other mechanisms such as magnetic dipole radiation. This will eventually lead to the synchronization of the two stars during the current low mass accretion phase. When accretion eventually switches on, once the M-star re-attaches to the Roche lobe, then AR Sco will become a synchronized magnetic cataclysmic variable, or polar, consisting of a highly magnetized white dwarf rotating synchronously with its M5 secondary companion.

**Magnetic field interactions.** It has been demonstrated[17] that mass-transferring secondary stars with orbital periods in the range $P_{orb} = 3-4$ h can have surface polar magnetic fields of the order of $B \approx 3,000$ G, which implies that the M5 secondary star of AR Sco will most probably be magnetically active. This is supported by MHD modelling in convective envelopes of dwarf stars[22]. This provides a mechanism for explaining the observed SED of AR Sco below $\nu \approx 10^{13}$ Hz in terms of magnetic energy dissipation in the field of the secondary star.

The field-aligned electric potentials in the M-star magnetic flux tubes are of the order of

$$\Phi_\parallel = \left( \frac{300(\Delta B_\perp)^3}{64\pi e n_e^{3/2} \sqrt{4\pi kT}} \right) \text{V} \tag{6}$$

$$\approx 200 \left( \frac{\Delta B_\perp}{700 \text{ G}} \right)^3 \left( \frac{n_e}{10^{10} \text{ cm}^{-3}} \right)^{-3/2} \left( \frac{T}{10^4 \text{ K}} \right)^{-1/2} \text{MV} \tag{7}$$

where we have assumed that $\Delta B_\perp \to B_{b1} \approx 700$ G represents the perturbation induced in the coronal loops, or flux tubes, of the secondary as a result of the white-dwarf field periodically pushing against it. These coronal structures will be periodically perturbed, pushed sideways by the rotating white-dwarf field and generating a 'fracture zone' which will induce large field-aligned potentials that can accelerate charged particles[26].

In these interactions, the magnetic pitch can increase $\gamma_\phi = (\Delta B_\perp/B) \to 10$ (see for example refs [44,45]) before the fields become unstable to reconnection. It should be mentioned that the magnetic field perturbation is still below the maximum magnetic field near the poles of the secondary, which can be of the order of 3,000 G (see for example ref. [17]). Electrons with energies of the order of $\gamma_e \leq 400$ trapped in pumped coronal fields of the order of $\langle B_{cor} \rangle \approx 100$ G (at a distance from the secondary surface of $\sim 2R_2$) will radiate synchrotron radiation at frequencies up to $\nu_{syn} \approx \gamma_e^2 eB/(2\pi m_e c) \leq 4 \times 10^{13}(\gamma_e/400)^2(B/100 \text{ G})$ Hz, in the infrared to radio regime.

**Pulsar-like particle acceleration.** For AR Sco, electrical potentials of the order

$$\Delta V \approx 10^{12} \left( \frac{P_{wd}}{117 \text{ s}} \right)^{-5/2} \left( \frac{\mu}{8 \times 10^{34} \text{ G cm}^3} \right) \left( \frac{R_*}{5.5 \times 10^8 \text{ cm}} \right) \text{V} \tag{8}$$

can be induced between the white dwarf and the light cylinder[29], where the white-dwarf magnetosphere co-rotates at the speed of light ($c = \omega_{wd} r_{lc}$). For AR Sco, the light cylinder radius is of the order of $r_{lc} \approx 6 \times 10^{11}(\omega_{wd}/0.054 \text{ rad s}^{-1})$ cm. Since this electric field is several orders of magnitude stronger than gravity, charged particles such as electrons can be pulled from the surface of the white dwarf and accelerated to relativistic energies[46], of the order of $\gamma_e \approx 10^6$, resulting in synchrotron emission up to frequencies of the order of

$$\nu_{syn} \approx 10^{18} \left( \frac{B_{1-c}}{0.4 \text{ G}} \right) \left( \frac{\gamma_e}{10^6} \right)^2 \text{Hz} \tag{9}$$

with peak emission occurring at $\nu_c \approx 0.3\nu_{syn} \approx 3 \times 10^{17}$ Hz, in the X-ray regime.

Additionally, outside the light cylinder, the fast-rotating magnetosphere will turn into a relativistic magnetohydrodynamic 'striped' wind (see refs [30–32], and references therein). It will consist of zones of opposite magnetic polarity that will form current sheets, which can be a source of particle acceleration through magnetic reconnection and pulsed incoherent synchrotron emission (see ref. [32] for a review). The emission will be pulsed as a result of a relativistic beaming effect due to these zones of opposite magnetic polarity that propagate outward at relativistic velocities ($v \to c$), separated by $\Delta l = \pi r_{lc}$ (here $r_{lc}$ is the light

cylinder radius). Each outward-propagating zone is beaming radiation into a forward cone of opening angle $\theta \approx 2/\gamma$, where $\gamma$ represents the wind Lorentz factor. Pulses will be observed when the time delay between emission on each expanding wavefront that intersects the observer (that is, $\Delta t \approx R/2\gamma^2 c$) is less than the time delay between the radiation from two successive outward-propagating wavefronts ($\Delta T = \Delta l/c$).

A characteristic of the synchrotron radiation from the striped wind outside the light cylinder radius is the fact that the toroidal magnetic field component oscillates in the same sense as the rotating pulsar, which results in pulsations at both the fundamental and first harmonic of the spin period. The emission is also expected to be polarized, emitting both linear and a small component of circular polarized light[32]. Applied to the Crab pulsar, numerical simulations of the expected pulse profiles produced by a striped wind exactly mimic the observed pulse profiles, together with the position angle swings through 180°. The observed polarized pulse profiles of AR Sco (Figs 3 and 4), especially near orbital phase $\Phi_o \approx 0.15$, mimic that of the Crab pulsar, perhaps implying that a striped pulsar wind is active in AR Sco. The fact that the striped wind occurs in a binary system may further introduce a beat frequency in the pulsations.

Both these processes, namely synchrotron emission in the vicinity of the light cylinder, or outside in the striped pulsar-like wind, can account for the nature of the polarized pulsed emission seen in optical light curves of AR Sco. Both processes can explain the polarization as a signature of synchrotron radiation, pulsed at both the white-dwarf spin period and the beat (synodic) period.

## References

1. Gold, T. Rotating neutron stars as the origin of the pulsating radio sources. *Nature* **218,** 731–732 (1968).
2. Marsh, T. R. *et al.* A radio-pulsing white dwarf binary star. *Nature* **537,** 374–377 (2016).
3. Wynn, G. A., King, A. R. & Horne, K. A magnetic propeller in the cataclysmic variable AE Aquarii. *Mon. Not. R. Astron. Soc.* **286,** 436–446 (1997).
4. Ikhsanov, N. R. The pulsar-like white dwarf in AE Aqarii. *Astron. Astrophys.* **338,** 521–526 (1998).
5. Meintjes, P. J. & Venter, L. A. The diamagnetic blob propeller in AE Aquarii and non-thermal radio to mid-infrared emission. *Mon. Not. R. Astron. Soc.* **360,** 573–582 (2005).
6. Oruru, B. & Meintjes, P. J. X-ray characteristics and the spectral energy distribution of AE Aquarii. *Mon. Not. R. Astron. Soc.* **421,** 1557–1586 (2012).
7. Potter, S. B. *et al.* Polarized QPOs from the INTEGRAL polar IGRJ14536-5522 (=Swift J1453.4-5524). *Mon. Not. R. Astron. Soc.* **402,** 1161–1170 (2010).
8. Słowikowski, A., Kanbach, G., Kramer, M. & Stefanescu, A. Optical polarization of the Crab pulsar: Precision measurements and comparison to the radio emission. *Mon. Not. R. Astron. Soc.* **397,** 103–123 (2009).
9. Karastergiou, A. & Johnston, S. Absolute polarization position angle profiles of southern pulsars at 1.4 and 3.1 GHz. *Mon. Not. R. Astron. Soc.* **365,** 353–366 (2006).
10. Radhakrishnan, V. & Cooke, D. J. Magnetic poles and the polarization structure of pulsar radiation. *Astrophys. J. Lett.* **3,** 225–229 (1969).
11. Landolfi, M., Landi Degl'Innocenti, E., Landi Degl'Innocenti, M. & Leroy, J. L. Linear polarimetry of Ap stars. I. A simple canonical model. *Astron. Astrophys.* **272,** 285–298 (1993).
12. Butters, O. W. *et al.* Circular polarization survey of intermediate polars. I. Northern targets in the range 17 h < RA < 23. *Astron. Astrophys.* **496,** 891–902 (2009).
13. Potter, S. B. *et al.* On the spin modulated circular polarization from the intermediate polars NY Lup and IGR J150946649. *Mon. Not. R. Astron. Soc.* **420,** 2596–2602 (2012).
14. de Búrca, D. & Shearer, A. Circular polarization of synchrotron radiation in high magnetic fields. *Mon. Not. R. Astron. Soc.* **450,** 533–540 (2015).
15. Ferrario, L., de Martino, D. & Gänsicke, B. T. Magnetic white dwarfs. *Space Sci. Rev.* **191,** 111–169 (2015).
16. Katz, J. I. AR Sco: A white dwarf synchronar. *Astrophys. J.* Preprint at https://arxiv.org/abs/1609.07172 (2017).
17. Meintjes, P. J. & Jurua, E. Secondary star magnetic fields in close binaries. *Mon. Not. R. Astron. Soc.* **372,** 1279–1288 (2006).
18. Becker, W. & Trümpher, J. The X-ray luminosity of rotation-powered pulsars. *Astron. Astrophys.* **326,** 682–691 (1997).
19. Becker, W. in *Neutron Stars and Pulsars* (ed. Becker, W.) 91–140 (Springer, 2009).

20. Abdo, A. A. *et al.* The first Fermi Large Area Telescope catalog of gamma-ray pulsars. *Astrophys. J. Suppl. Ser.* **187,** 460–494 (2010).
21. Geng, J.-J., Zhang, B. & Huang, Y.-F. A model of white dwarf pulsar AR Scorpii. *Astrophys. J.* **831,** L10 (2016).
22. Donati, J.-F. & Landstreet, J. D. Magnetic fields of nondegenerate stars. *Annu. Rev. Astron. Astrophys.* **47,** 333–370 (2009).
23. Mestel, L. Magnetic braking by a stellar wind I. *Mon. Not. R. Astron. Soc.* **138,** 359–391 (1968).
24. Mestel, L. & Spruit, H. C. On magnetic braking of late-type stars. *Mon. Not. R. Astron. Soc.* **226,** 57–66 (1987).
25. Haerendel, G. Acceleration from field-aligned potential drops. *Astrophys. J. Suppl. S.* **90,** 765–774 (1994).
26. Venter, L. A. & Meintjes, P. J. The tenuous X-ray corona enveloping AE Aquarii. *Mon. Not. R. Astron. Soc.* **378,** 681–690 (2007).
27. van der Laan, H. A model for variable extragalactic radio sources. *Nature* **211,** 1131–1133 (1966).
28. Bastian, T. S., Dulk, G. A. & Chanmugam, G. Radio flares from AE Aquarii: A low-power analog to Cygnus X-3? *Astrophys. J.* **324,** 431–440 (1988).
29. Arons, J. & Scharlemann, E. T. Pair formation above polar caps — structure of the low altitude acceleration zone. *Astrophys. J.* **231,** 854–879 (1979).
30. Michel, F. C. Coherent neutral sheet radiation from pulsars. *Comments Astrophys. Space Phys.* **3,** 80–86 (1971).
31. Coroniti, F. V. Magnetically striped relativistic magnetohydrodynamic winds: The Crab nebula revisited *Astrophys. J.* **349,** 538–545 (1990).
32. Kirk, J. G., Lyubarsky, Y. & Pétri, J. in *Neutron Stars and Pulsars* (ed. Becker, W.) 421–450 (Springer, 2009).
33. Patterson, J. The DQ Herculis stars. *Publ. Astron. Soc. Pacif.* **106,** 209–238 (1994).
34. Meintjes, P. J. On the evolution of the nova-like variable AE Aquarii. *Mon. Not. R. Astron. Soc.* **336,** 265–275 (2002).
35. Schenker, K., King, A. R., Kolb, U., Wynn, G. A. & Zhang, Z. AE Aquarii: How cataclysmic variables descend from supersoft binaries. *Mon. Not. R. Astron. Soc.* **337,** 1105–1112 (2002).
36. Potter, S. B. *et al.* Polarized QPOs from the INTEGRAL polar IGRJ14536-5522 (=Swift J1453.4-5524). *Mon. Not. R. Astron. Soc.* **402,** 1161–1170 (2010).
37. Hsu, J.-C. & Breger, M. On standard polarized stars. *Astrophys. J.* **262,** 732–738 (1982).
38. Eastman, J., Siverd, R. & Gaudi, S. Achieving better than 1 minute accuracy in the heliocentric and barycentric Julian dates. *Publ. Astron. Soc. Pacif.* **122,** 935–946 (2010).
39. Paczynski, B. Evolution of single stars. VI. Model nuclei of planetary nebulae. *Acta Astron.* **21,** 417–435 (1971).
40. Plavec, M. & Kratochvil, P. Tables for the Roche model of close binaries. *Bull. Astr. Czech.* **15,** 165–170 (1964).
41. Joss, P. C., Katz, J. I. & Rappaport, S. A. Synchronous rotation in magnetic X-ray binaries. *Astrophys. J.* **230,** 176–183 (1979).
42. Papaloizou, J. & Pringle, J. E. A model for VW Hydri. *Astron. Astrophys.* **70,** L65–67 (1978).
43. Campbell, C. G. in *Magnetohydrodynamics in Binary Stars* 88–89 (Kluwer, 1997).
44. Ghosh, P & Lamb, F. K. in *Neutron Stars: Theory and Observation* (eds Ventura, J. E. & Pines, D.) 363–444 (Kluwer, 1991).
45. Meintjes, P. J. & de Jager, O. C. Propeller spin-down and non-thermal emission from AE Aquarii. *Mon. Not. R. Astron. Soc.* **311,** 611–620 (2000).
46. Goldreich, P. & Julian, W. H. Pulsar electrodynamics. *Astrophys. J.* **157,** 869–880 (1969).

## Acknowledgements

## Author contributions

D.A.H.B. conceived the HIPPO observing programme, organized and undertook the observations, assisted in the analysis and interpretation of the polarimetry, participated in the modelling and was primary author of the paper. P.J.M. undertook the modelling and led most of the interpretation. S.B.P. undertook the reductions of the HIPPO data, produced most of the figures and assisted in interpretation of the results. T.R.M. and B.T.G. provided information on AR Sco, including pre-publication material, and assisted in the interpretation of the results and models.

## Additional information

**Supplementary information** is available for this paper.

**Reprints and permissions information** is available at www.nature.com/reprints.

**Correspondence and requests for materials** should be addressed to D.A.H.B.

**How to cite this article:** Buckley, D. A. H. *et al.* Polarimetric evidence of a white dwarf pulsar in the binary system AR Scorpii. *Nat. Astron.* **1,** 0029 (2017).

## Competing interests

The authors declare no competing financial interests.